Moose Project

Part 1

Vaughn Ramsey

February 2025

1 Setup and Mesh Refinement

To start building our mesh we consider the basics of the problem. We recognize that it is important to have nodes located at the interface of each material and on the corners of our model. To achieve this we define 3 generated meshes, one on the domain $x \in [0, 0.5], y \in 0, 0.1$ for the fuel, one on $x \in [0.5, 0.505], y \in [0, 0.1]$ for the gap, and one on $x \in [0.505, 0.605], y \in [0, 0.1]$. We start meeting the minimum mesh requirements with an n_x of 3, which yields one solid block on each subdomain. Then we use the stitched mesh generator to combine our generated meshes, and finally the subdomain bounding box generator to redefine out subdomains that were lost in the stitching. This yields the mesh we see in the simulation depicted in Fig. 1.

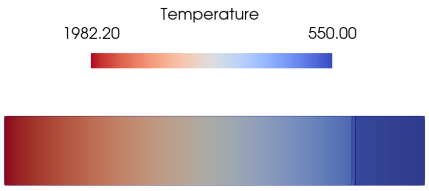

Figure 1: Heat map for simulated fuel rod with $n_x = 3$

[H] We can clearly see that the heat is almost uniformly diffusing across the fuel element. To resolve this numerical inaccuracy, we need to refine our mesh. In order to systematically control the mesh refinement process, I incrementally increased the number of subdivisions uniformly across each component, such that for $n_x = 9$, there are three nodes across the fuel, three across the gap, and three across the clad. Through this process, I began slowly increasing the number of subdivisions, then taking larger steps as convergence slowed, until we reached a sufficiently small change in center line temperature between iterations in mesh refinement. The general refinement process can be seein in Fig. 2. This ultimately yielded a change in temperature of $\Delta T_0 = 0.04^o K$ for an increase of

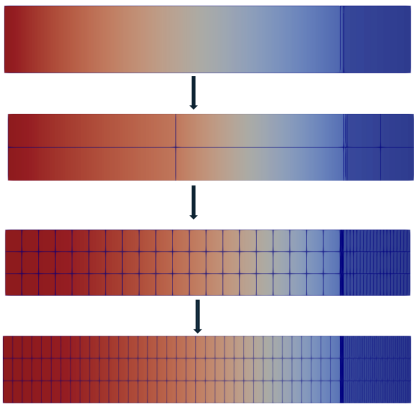

Figure 2: Abstracted flowchart of the mesh refinement process.

1 in n_x. We reached this tolerance at $n_x = 105$, or 35 subdivisions across each material (i.e. fuel, gap, clad). See a plot of our convergence by ΔT_0 vs n_x in Fig. 3.

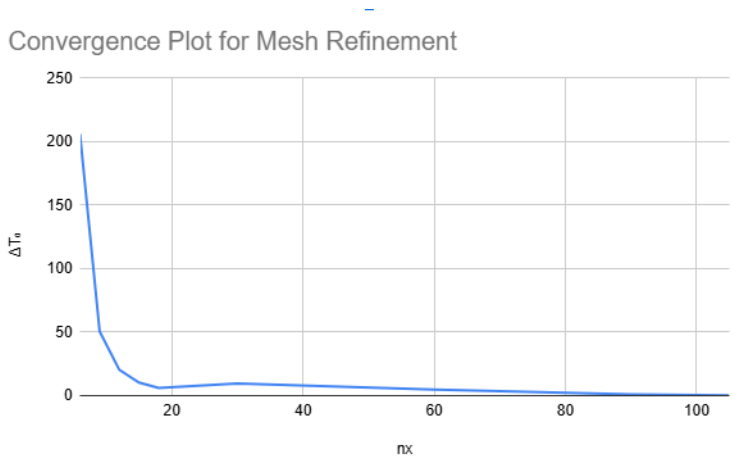

Figure 3: Convergence plot of change in center-line temperature as mesh is refined.

Not having a specified tolerance, I chose to stop here, as further refinement slowed the convergence of our thermal conductivity solver without yielding large improvements in calculated center-line temperature. Finally we assign thermal conductivity values to our subdomains through heat conduction materials with the values seen in Table 1.

Material	Thermal Conductivity (W/cm·K)
Fuel	0.03
Gap	0.004
Cladding	0.18

Table 1: Thermal conductivity values for nuclear fuel, gap, and cladding.

2 Steady State Simulation

For the steady state implementation the heat conduction kernel is used and all materials are defined as heat conduction materials. The heat source kernel is also defined by a volumetric heat generation rate, derived from an LHR of $350[\frac{\mathrm{W}}{\mathrm{cm}}]$. Dirichlet and Neumann boundary conditions are also implemented with a temperature $T = 550^o\mathrm{C}$ at the rightmost boundary as described in the problem statement and $\frac{\delta T}{\delta x} = 0$ at the left most nodes, respectively.

2.1 Analytical Solution

Recall the equations from our first unit for calculating the temperature drop over media and fuel:

$$T_0 - T_1 = \frac{\mathrm{LHR}}{2\pi R_\mathrm{f}} \frac{t}{k} \tag{1}$$

$$T_0 - T_s = \frac{\mathrm{LHR}}{4\pi k} \tag{2}$$

With these equations we go ahead and begin the analytical solve, starting with the temperature drop over the cladding:

$$\begin{aligned} T_\mathrm{IC} - T_\mathrm{OC} = \frac{350}{2\pi \cdot 0.5} \frac{0.1}{0.18} &\approx 61.89^o[\mathrm{K}] \\ T_\mathrm{IC} &\approx 611.89^o[\mathrm{K}] \\ T_\mathrm{S} - T_\mathrm{IC} = \frac{350}{2\pi \cdot 0.5} \frac{0.005}{0.004} &\approx 139.26^o[\mathrm{K}] \\ T_\mathrm{S} &\approx 751.15^o[\mathrm{K}] \\ T_0 - T_\mathrm{S} = \frac{350}{4\pi \cdot 0.03} &\approx 928.4^o[\mathrm{K}] \\ T_0 &\approx 1679.56^o[\mathrm{K}] \end{aligned}$$

Having examined the analytical temperature profile, let's take a look at the simulated one.

2.2 Computational Results

To begin our computational analysis we must first convert from LHR to a volumetric heating rate q. To convert to a volumetric format we divide the LHR

by the cross-sectional area of our fuel pellet:

$$q = \frac{\text{LHR}}{\pi R_{\text{fuel}}^2} = 445.63$$

Within our moose code we define the heat source kernel to operate with this volumetric heating rate and only in the fuel subdomain. Having fully set up our mesh and kernels we run the simulation which outputs the following heat map:

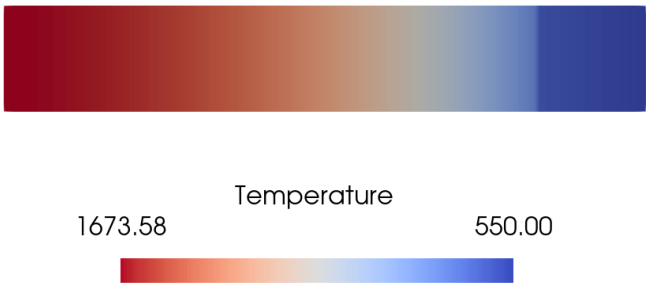

Figure 4: 1-D heat map for the radial cross section of the fuel pellet.

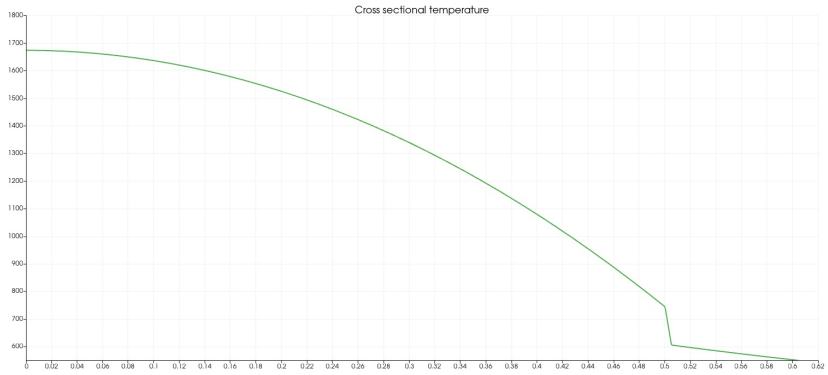

Figure 5: Cross sectional graph of temperature vs radius with temperature labels at the interior of the cladding and surface of the fuel $n_x = 105$.

The heat map in Fig. 4. depicts the thermal gradient across the fuel element, and the plot in Fig. 5. depicts the cross-sectional plot of temperature vs radius depicted in the map. We do not implement a time derivative kernel because our solid state simulation does not need to account for the heating of the fuel.

2.3 Comparison

Referring to Fig. 4. and Fig. 5 we can see the simulated values at key points in the analytical solve we did in 2.1. We see that T_{IC} was quite close and had

a 0.98% error relative to the analytical result, T_S was similarly close having a 0.89% error relative to the analytical solution. Finally T_0 had a percent error of 0.35% relative to our analytical solve. This alignment reaffirms the efficacy of our MOOSE model. We also find that error must propogate somewhat constantly through the model given that the $\Delta T \approx 6^o$[K] at each interface.

3 Transient Simulation

3.1 Transient Solver Parameters

For the transient simulation we use the mesh that resulted from our refinement study in Section 1.

3.2 Constant Thermal Conductivity

In the case of a constant thermal conductivity we keep our values from the steady state simulation. Implementing the transient we use the given equation:

$$\text{LHR} = 350 \cdot e^{-\frac{(t-20)^2}{2}} + 350$$

Recalling that our heat generation kernel works from volumetric heat generation we again divide our LHR formula by the cross sectional area of the fuel pellet.

$$Q = \frac{350 \cdot e^{-\frac{(t-20)^2}{2}} + 350}{R_{\text{fuel}}^2 \pi} = \frac{350 \cdot e^{-\frac{(t-20)^2}{2}} + 350}{0.25\pi}$$

We simply define a function for heat generation and give this function as the source for the heat generation kernel. Given that we are no longer in a steady state simulation, we must also define a specific heat capacity and density for each material. The assigned values are shown in Table 2. After adding these

Material	**Specific Heat (J/kg·K)**	**Density (kg/cm^3)**
UO_2 (Fuel)	296.7	0.01097
Helium (Gap)	5190	0.000000164
Zircaloy-4 (Cladding)	2850	0.00656

Table 2: Utilized specific heat and density values for UO_2 (fuel), helium (gap), and Zircaloy-4 (cladding).

material properties to each block in the code, we find that our fuel now needs time to heat up, find a graph of center-line temperature over time in Fig.

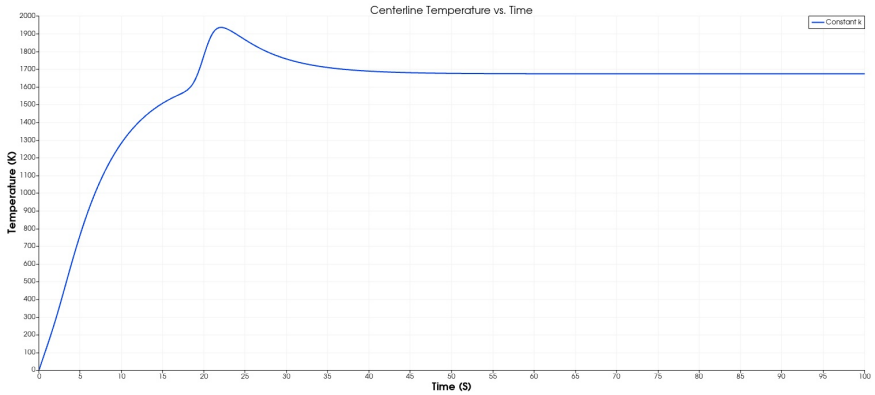

Figure 6: Center-line temperature vs time in transient with constant thermal conductivity.

We find that the system achieves a maximum temperature at $t = 21.9$[s] with a center-line temperature $T_0 = 1855.94$[K]. After attaining a maximum temperature it declines back to a steady state solution. The final center-line temperature at $t = 100$[s] is $T_0 = 1673.62^o$[K]. This is super close to the center-line temperature that our steady state mesh refinement study converged to and close to the analytically found center-line temperature, reaffirming the validity of our model.

3.3 Temperature Dependent Thermal Conductivity

We define our temperature-dependent thermal conductivity function as seen in Table 3.

Material	Thermal Conductivity Model (W/cm·K)	Reference
UO_2	$k = \frac{1}{2(1.48+0.04\max(T,300))}$	OECD UO_2 Model
Helium	$k = 0.0025 + 0.00002T$	Approximate helium gas $k(T)$
Zircaloy-4	$k = 0.18 - 0.00002T$	Zircaloy-4 $k(T)$ Model

Table 3: Temperature-dependent thermal conductivity models for UO_2, helium, and Zircaloy-4. Temperature (T) is in Kelvin.

These functions were defined in the functions block and referenced in each heat conduction material's thermal conductivity temperature function. Auxiliary variables and kernels were set up so that the thermal conductivity can be checked at different points in the material and at different times. Implementing these parameters yielded the center-line temperature vs. time plot seen in Fig. 7.

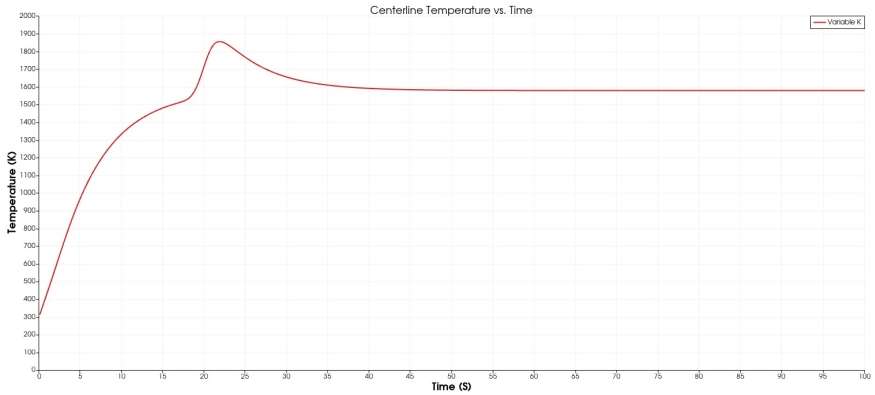

Figure 7: Center-line temperature vs. time in temperature dependent thermal conductivity regime.

In this model we find that the center-line reaches a maximum temperature at $t = 22$[s] with a $T_0 = 1935.01$[K]. The implementation of the functions in Table 3 necessitates a nonzero starting temperature for the fuel, so we begin with the fuel at 300^o[K]. We observe a similar behavior to the case of constant thermal conductivity with a heating behavior interrupted by the transient.

3.4 Comparison

We may visually compare the results of the constant thermal conductivity with the temperature-dependent conductivity to better understand the different behaviors (see Fig. 8.)

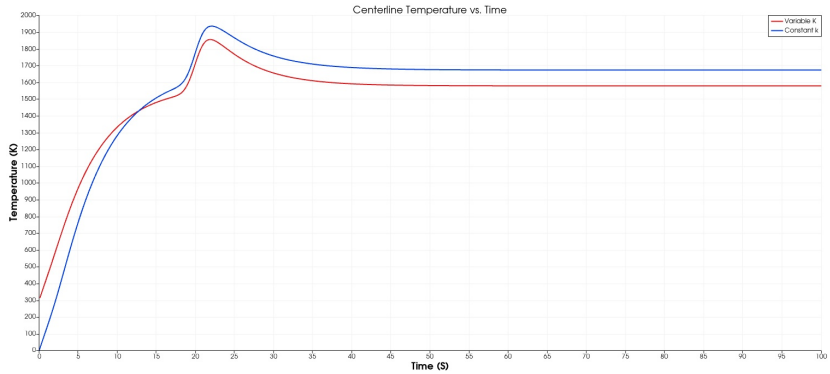

Figure 8: Plot with center-line temperature of fuel during transient with both constant and temperature dependent thermal conductivity values.

The final center-line temperature at $t = 100$[s] is $T_0 = 1579.11$. The discrepancy between the final behavior of T_0 in the constant and temperature

dependent thermal conductivity cases is attributed to the fact that our thermal conductivity models do not exactly match the constant thermal conductivities at our operating temperatures.

4 Conclusion

In this project we simulated the temperature profile and heating behavior of a 1-D cross section of a nuclear fuel rod assuming a constant outer cladding temperature of 550^o[K]. We performed mesh refinement in the steady-state case and then over a heat production transient. We implemented the transient case with both constant and temperature dependent thermal conductivity. The constant thermal conductivity case we found results that aligned quite will with the analytical solution. In the case of temperature dependent thermal conductivity we found significantly different center-line temperatures, but they were still within reason. To take this project further one could refine the thermal conductivity models such that they have the same thermal conductivity values at our operating temperatures as the constant thermal conductivity values. Temperature dependent specific heat functions could also be implemented, as well as thermal expansion.